Polymer Chemistry

Design, Synthesis and Characterization of Fused Bithiazole- and Dithiophene-Based Low Bandgap Thienylenevinylene Copolymers

Journal:	*Polymer Chemistry*
Manuscript ID	PY-ART-06-2021-000773.R1
Article Type:	Paper
Date Submitted by the Author:	24-Aug-2021
Complete List of Authors:	Patra, Dhananjaya; Texas A&M University at Qatar, Chemistry Comi, Marc; Texas A&M University at Qatar Zhang, Xianhe ; Southern University of Science and Technology Kini, Gururaj; Konkuk University, ; Udayakantha, Malsha; Texas A&M University, Department of Chemistry Kalin, Alexander; Texas A&M University, Chemistry Banerjee, Sarbajit; Texas A&M University, Department of Chemistry Fang, Lei; Texas A&M University, Chemistry; Texas A&M University, Materials Science and Engineering Guo, Xugang; Southern University of Science and Technology, Al-Hashimi, Mohammed; Texas A&M University at Qatar,

ARTICLE

Design, Synthesis and Characterization of Fused Bithiazole- and Dithiophene-Based Low Bandgap Thienylenevinylene Copolymers

Received 00th January 20xx,
Accepted 00th January 20xx

DOI: 10.1039/x0xx00000x

Dhananjaya Patra,‡[1] Marc Comí,‡[1] Xianhe Zhang,[2] Gururaj P. Kini,[3] Malsha Udayakantha,[4] Alex Kalin,[4] Sarbajit Banerjee,[4] Lei Fang,[4] Xugang Guo[2] and Mohammed Al-Hashimi[1]*

ABSTRACT: The structural rigidity of fused units in the polymer backbone, in addition to the resulting stabilizing effect of the quinoidal structure, and tunable electronic properties has played a key role in promoting highly-ordered π-stacking moieties, exhibiting promising charge carrier mobilities. The electron-deficient thiazole moiety shows high planarity and effective π-π stacking, which leads to the reduction in the energy levels of the highest occupied and lowest unoccupied molecular orbitals (HOMO/LUMO), and ideally enhances the electron charge mobility. Four heterocycle-based monomers **BTzS**, **BTzSe**, **DTS**, and **DTG** based on the fused bithiazole and dithiophene units incorporated with sulfur, selenium, silicon, and germanium as the bridging atoms were synthesized and characterized. The monomers were copolymerized with the electron-rich alkylated thienylenevinylene (TV) unit to afford copolymers **P1-P4**. The thermal, optical, and electrochemical properties, and crystallinity of the copolymers was thoroughly investigated. Extensive OFET device optimization using different solvents and annealing temperatures resulted in the best charge mobility of 0.09 cm^2/Vs for the electron deficient bithiazole **BTzS** copolymer **P1** and 0.36 cm^2/Vs for the **DTS** copolymer **P3**.

Introduction

The synthesis of π-conjugated small molecules and polymers has attracted significant attention in the last few decades, due to their flexible fabrication, cost-effectiveness, and large-area production in optoelectronic devices.[1-8] Considerable effort has been directed towards designing new conjugated building blocks, developing novel fabrication strategies, and advancing device engineering, which has resulted in a significant increase in charge-carrier mobilities of organic field-effect transistors (OFETs).[9-13] Several strategies have been utilized in designing low-bandgap π-conjugated polymeric semiconductors that exhibit high mobility. In principle, they are based on either suppressing the angular torsions through planarization of the backbone,[14, 15] maintaining high crystallinity,[16, 17] and/or by having a combination of electron-rich and electron-deficient units that alternate across the polymer backbone.[18-23] Widely used electron-deficient building block are monomers containing an electron-withdrawing nitrogen atom within the ring, such building blocks include thiazoles, thiadiazoles, cyclic amides, cyclic imides and their fused derivatives.[24-26]

Dithieno[3,2-b:2',3'-d]thiophene (DTT) unit is one of the many building blocks that has played a key role in promoting highly-ordered π-stacking and exhibiting high hole mobilities. This is attributed to its structural rigidity in the fused polymer backbone, the stabilizing effect of the quinoidal structure, S–S interactions, and its tunable electronic properties.[27-29] Replacing the thiophene units with the electron-deficient thiazole moiety would lead to the reduction in the energy levels of the highest occupied and lowest unoccupied molecular orbitals (HOMO/LUMO), and ideally enhance the electron charge mobility.[30-33] In addition, incorporating different chalcogen atoms such as selenium, or d-block atoms such as silicon or germanium to bridge the thiazole units will afford the fused building block and further improve charge transport.[34-39] Several dithiophene fused-copolymers such as dithienosilole (**DTS**)[40-43] and dithienogermole (**DTG**)[44-48](**Figure 1**), have been utilized as electron-rich donors, exhibiting maximum charge mobilities up to 0.19 cm^2/Vs [49-53] and 0.11 cm^2/Vs, respectively.[54, 55]

Alkylated thienylenevinylene (TV) electron-rich moieties have been widely used in the polymer backbone to prevent angular torsion, which results in coplanar structures, ensures facile solubility while retaining extended π-conjugation, and engendering electronic gains towards bandgap energy modulation.[56-58] As such, the polymers exhibit reduced energy bandgaps and higher hole mobilities, as a result of enhanced interchain interactions.

Our group has previously shown the synthesis of various polymers based on pyrrolebithiazole (PBTz) with the TV unit (**Figure 1**) to

[1] Department of Chemistry, Texas A&M University at Qatar, Education City, Doha, P.O. Box 23874, Qatar.
[2] Department of Materials Science and Engineering, Southern University of Science and Technology (SUSTech), No. 1088, Xueyuan Road, Shenzhen, Guangdong 518055, China
[3] Nano and Information Materials (NIMs) Laboratory, Department of Chemical Engineering, Konkuk University, 120, Neungdong-ro, Gwangjin-gu, Seoul 05029, Korea.
[3] Department of Chemistry, Texas A&M University, College Station, TX 77843-3012, United States.
‡ These authors contributed equally.

*Corresponding Author: **mohammed.al-hashimi@tamu.edu**

Supporting Information: Information on general experimental details, synthetic procedures, polymerization, characterization, and spectroscopic data.

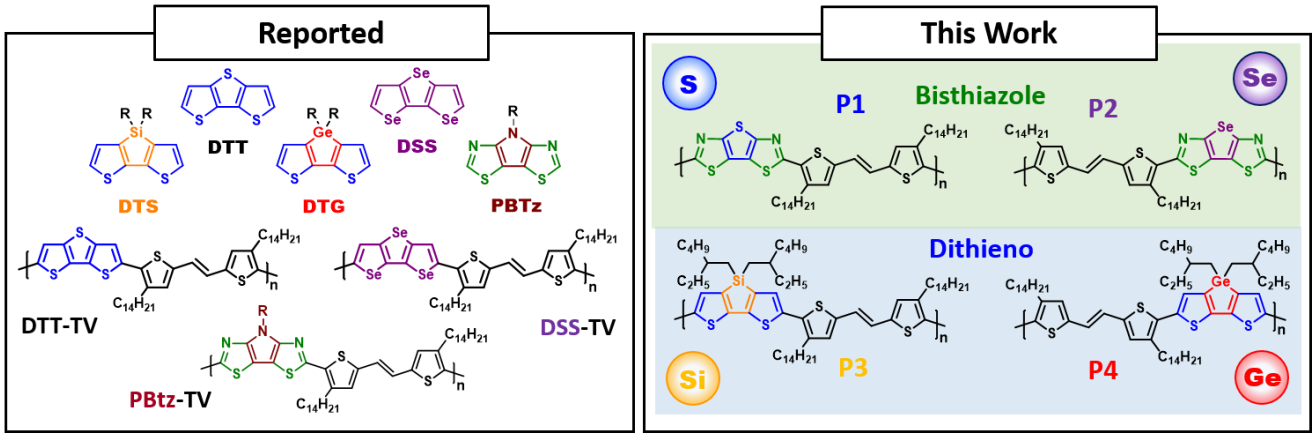

Figure 1. Chemical structures of relevant previous and the current work of fused dithiophene and bithiazole derivatives.

induce strong π–π stacking, and as a result have favourable molecular conformations.[59] In addition, Kim and co-workers have demonstrated that DTT based TV-copolymers with small angular torsion yield a planar conjugated system, thus promoting the delocalization of charge carriers exhibiting very high mobilities.[57] Recently, Heeney, Kim, and co-workers reported the synthesis of diseleno-selenophene (DSS)-TV copolymer (**Figure 1**). The copolymer demonstrated very strong intermolecular interaction in solution, and exhibited extremely high hole mobilities.[34]

Herein, we report the design, synthesis and characterisation of four copolymers **P1-P4**. Fused bithiazole and dithiophene units were incorporated with different bridging atoms, such as sulfur, selenium, silicon, and germanium. The monomers were copolymerized with the corresponding alkylated-TV unit to afford thieno[2,3-d:5,4-d']bithiazole (**P1**), selenopheno[2,3-d:5,4-d']bithiazole (**P2**), silolo[3,2-b:4,5-b']dithiophene (**P3**) and germolo[3,2-b:4,5-b']dithiophene (**P4**) as depicted in **Figure 1**. The thermal, optical, and electrochemical properties, and crystallinity of the copolymers have been investigated. Extensive OFET device optimization using different solvents and annealing temperatures afforded maximum charge mobilities for the electron deficient bithiazole copolymer **P1** to be 0.09 cm^2/Vs and for the DTS copolymer **P3** was 0.36 cm^2/Vs. To the best of our knowledge the mobilities obtained are the highest reported to date for these types of systems.

Results and Discussion

Synthesis, Characterization, and Thermal Properties.

The synthetic route to the four fused heterocycle-based monomers **BTzS**, **BTzSe**, **DTS,** and **DTG** is depicted in **Scheme 1**. 4,4'-dibromo-2,2'-bis(triisopropylsilyl)-5,5'-bithiazole **1** was reacted with bis(tributyltin)-sulfide or -selenide via Stille cross-coupling reaction in toluene to afford thieno- or selenopheno- [2,3-d:5,4-d']bi(thiazole) intermediates **2** and **3** in good yields.[60] The deprotection of **2** and **3** using tetra-*n*-butylammonium fluoride (TBAF) in tetrahydrofuran (THF) afforded compounds **4** and **5**, respectively. Subsequent bromination with NBS in DMF afforded the desired target monomers **BTzS** and **BTzSe** in 74-77% yield. Monomers **DTS** and **DTG** (Scheme 1b) were prepared by reacting dichloro*bis*(2-ethylhexyl)-silane or -germane precursors obtained from the reaction of (2-ethylhexyl)magnesium bromide with silicon- or germanium-tetrachloride.[61] Triisopropylsilane-protected dibromobithiophene monomer **6** was reacted with dichloro*bis*(2-ethylhexyl)-silane or -

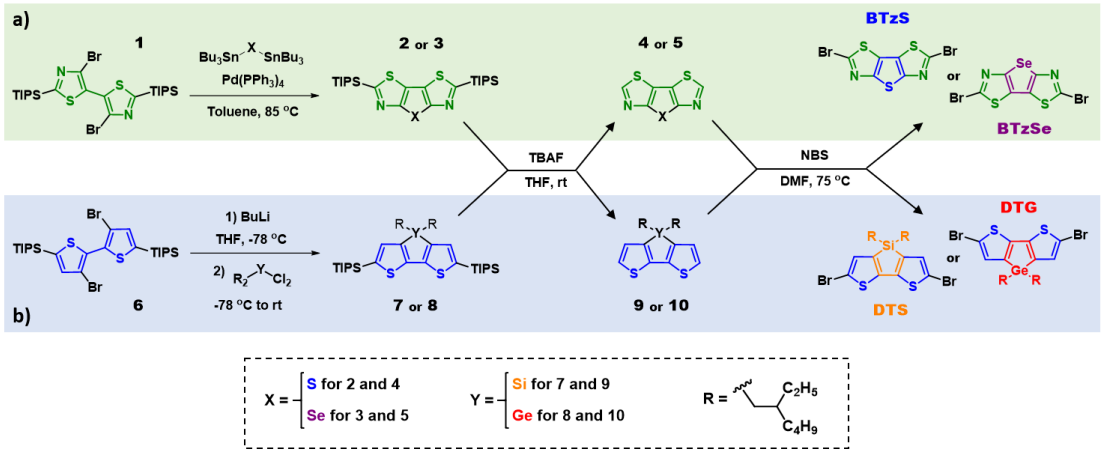

Scheme 1. Synthetic route to monomers a) **BTzS** and **BTzSe**, b) **DTS** and **DTG**.

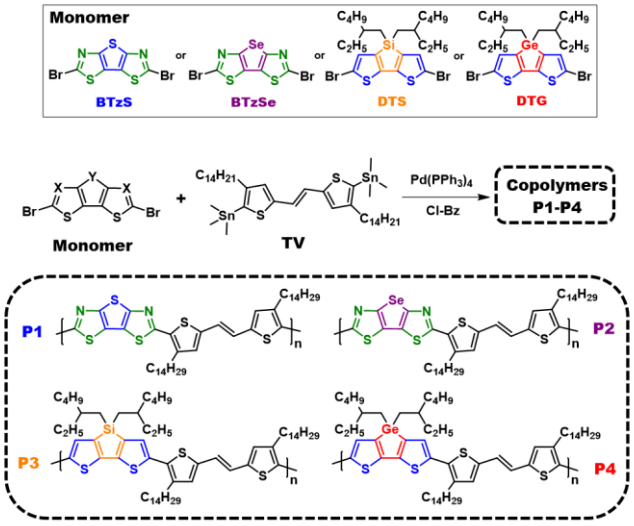

Scheme 2. Synthesis of **P1-P4** copolymers

germane to afford the alkylated silicon- or germanium -dithiophene derivatives **7** and **8**. Consequently, deprotection with TBAF, followed by bromination using NBS afforded the desired monomers **DTS** and **DTG** in 66-70% yield.[39, 55]

As depicted in **Scheme 2**, copolymers **P1-P4** were synthesized in a microwave reactor using Stille cross-coupling polymerization of monomers **BTzS, BTzSe, DTS,** and **DTG** with trimethyltin- (E)-2-[2-(thiophen-2-yl)-vinyl]thiophene (TV) in chlorobenzene using $Pd(PPh_3)_4$ as the catalyst. All copolymers were precipitated in acidified-methanol and purified by Soxhlet extraction with a sequence of refluxing in methanol, acetone, dichloromethane, and chloroform. After the samples were freed from any catalyst and small oligomeric residues, the copolymers were collected by reprecipitation in methanol. Copolymers **P1-P4** were isolated as dark purple solids and exhibited good solubility in chloroform (**Figure S1-S4**). Number average molecular weights (M_n) and polydispersity's ($Đ$) of the copolymers were measured by size-exclusion chromatography (SEC) in chlorobenzene using polystyrene as the standard (**Table 1**). Copolymers **P1-P4** exhibited molecular weights in the range of M_n = 21-38 kDa mol^{-1} with $Đ$ of 1.9-2.1. As a result of the lack in the solubilizing alkyl side chains in monomers **BTzS** and **BTzSe**, copolymers **P1** and **P2** had lower M_n in comparison with **P3** and **P4**.

Thermal properties of the copolymers were studied using thermogravimetric analysis (TGA) and differential scanning calorimetry (DSC) under a nitrogen atmosphere. As depicted in **Figure S5a** and **Table 1**, the copolymers **P1-P4** exhibited a wide range of thermal stability with onset decomposition temperatures (T_d) corresponding to 5% weight loss in the range of 393-400 °C for **P1** and **P2**, while the T_d for **P3** and **P4** was relatively lower at 331 °C. This can be attributed to the loss of the branched alkyl side chains attached to the Si and Ge bridge atoms, which pertains to an identical first decomposition at 331 °C with a weight loss of 15% observed in the first derivative curves for **P3** and **P4**. Thermal glass transition state in the DSC curves (**Figure S5b**) can be seen for all the copolymers ranging from 220 to 230 °C.

Optical Properties.

The UV-Vis absorption spectra of **P1-P4** in dilute chloroform solution and as spin-coated thin-film on quartz substrate are depicted in **Figure 2a-b**. Optical parameters, such as, maximum absorbance (λ_{max}) in solution and solid-state and the optical bandgap (E_g^{opt}) calculated from the onsets of the absorption spectra in thin-films of the copolymers **P1-P4** are summarized in **Table 1**. Copolymers based on the fused bithiazole system, **P1** and **P2**, exhibit a main π-π* transition with absorption maxima in chloroform solution/thin-film at 546/548 nm for **P1** and at 557/580 nm for **P2**. Upon going from solution to thin-film, the maximum absorption of both copolymers are red-shifted, and the absorption spectra present a distinctive shoulder at 631 nm for **P1** and 643 nm for **P2**, due to the strong intermolecular interactions in the solid-state. Additionally, the exchange of the chalcogen atom from sulfur to selenium in the bithiazole-based copolymers **P1** and **P2**, leads to a bathochromic shift of λ_{max} in solution and in thin-film by 11 and 32 nm, respectively.[62, 63] On the other hand, dithiophene-based copolymers **P3** and **P4** presented a λ_{max} in solution in the range of 560-566 nm, while the λ_{max} in thin-film was 592 nm for **P3** and 595 nm for **P4**, with strong vibronic shoulders at 645 nm for **P3** and 650 nm for P4.[64]

Table 1. Summary of molecular weights, thermal, optical, electrochemical, and GIWAXS parameters of copolymers **P1-P4**.

	[a]Mn (kDa)	Đ	Td (°C)	Tg (°C)	[b]λ_{max}^{sol} (nm)	[c]λ_{max}^{film} (nm)	[d]HOMO (eV)	[d]LUMO (eV)	[e]E_g^{el} (eV)	[f]E_g^{opt} (eV)	[g]Lamelar d^d (Å)	[g]π-π* d^d (Å)
P1	24	2.0	400	220	546	548	-5.38	-3.61	1.77	1.71	11.86	3.67
P2	21	1.9	393	224	557	580	-5.34	-3.59	1.75	1.70	11.52	4.27
P3	36	2.1	331	230	560	592	-5.42	-3.54	1.69	1.74	6.28	3.65
P4	38	2.1	331	222	566	595	-5.18	-3.56	1.62	1.67	5.61	3.61

[a] Determined by gel permeation chromatography (against polystyrene standards) in chlorobenzene at 85 °C. [b] λ_{max} in chlorobenzene dilute solution. [c] Spin-coated from chloroform solution onto a glass surface. [d] E_{HOMO}/E_{LUMO} = [−(E_{onset} − E_{onset} (FC/FC+ vs Ag/Ag+)) − 4.8] eV, where 4.8 eV is the energy level of ferrocene below the vacuum level and the formal potential E_{onset}(FC/FC+ vs Ag/Ag+) is equal to 0.48 V. [e] Electrochemical bandgap: E_g^{el} = $E_{ox/onset}$ − $E_{red/onset}$. [f] Optical bandgap: E_g^{opt} = 1240/λ_{edge}. [g] Calculated by d=2π/q (Å).

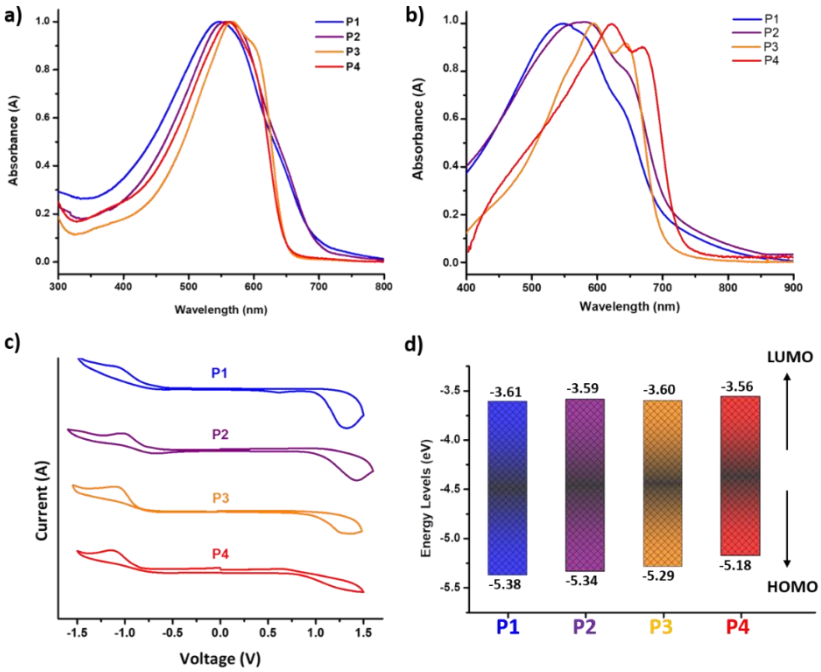

Figure 2. UV-vis absorption spectra of (a) 10^{-4} M solutions, and (b) thin films (on quartz substrates) of copolymers **P1-P4.** (c) Cyclic voltammograms of **P1-P4** thin-films (scan rate 50 mV s^{-1}), (d) HOMO and LUMO energy levels of the copolymers.

Copolymer **P3** displayed a red shift of 32 nm going from solution to film, in comparison with **P4** which was slightly lower (29 nm). A similar bathochromic effect is observed when changing the central atom from silicon (**P3**) to germanium (**P4**) in dithiophene-fused units, as have been observed in previously reported conjugated polymers.[48, 65] The optical band gaps (E_g^{opt}) for the copolymers **P1-P3** were estimated to be in the range of 1.70-1.74-eV, while the dithienogermole copolymer (**P4**) was relatively lower at 1.67 eV.

Electrochemical Properties.

The oxidation and reduction potentials of **P1-P4** were determined using cyclic voltammetry (CV) with ferrocene (Fc/Fc*) as an internal standard, as shown in **Figure 2c**. Copolymers **P1-P4** all exhibited pronounced oxidation and reduction bands with onset oxidation/reduction potentials (E_{ox} and E_{red}) at 1.04/-0.73, 1.00/-0.75, 0.95/-0.74, and 0.84/-0.78 eV for **P1**, **P2**, **P3**, and **P4**, respectively. The HOMO and LUMO energy levels were calculated based on the onset of the first E_{ox} and E_{red} potentials in comparison to the Fc/Fc* oxidation/reduction potential under vacuum of -4.8 eV as summarized in **Table 1**. The HOMO/LUMO energy levels of **P1-P4** were estimated to be -5.38/-3.61 (**P1**), -5.34/-3.59 (**P2**), -5.29/-3.60 (**P3**), and -5.18/-3.56 eV (**P4**), as shown in **Figure 2d**. We observed by changing the chalcogen atom from sulfur to selenium (**P1** to **P2**) in the fused bithiazole systems or from silicon to germanium (**P3** to **P4**) in the dithiophene system, the HOMO energy levels become more stabilized. Thus, as a result of increasing the size of the bridge central atom for both systems leads to higher HOMO energy levels. Similarly, subtle differences in the LUMO energy levels were also observed going from **P1** to **P2** (-3.61 to -3.59 eV), as a result of the chalcogen atom substitution. For the fused dithiophene-based copolymers when substituting the Si atom in **P3** with the larger bridge Ge atom in **P4**, the LUMO energy level was slightly stabilized by -0.06 eV. Fused thiophene DTT-TV (Figure 1) based-copolymers[29, 66] are reported to exhibit a strong oxidation band with estimated HOMO energy level at -4.80 eV, suggesting its high donor character, which is promoted by the continuous presence of electron-rich moieties in the copolymer main chain. In comparison, copolymer **P1** which contains the electron-deficient fused bithiazole moiety, displayed clear oxidation and reduction bands. As a result, the deeper-lying LUMO energy levels of bithiazole-containing copolymers **P1** and **P2** are seen to be directly influenced by the electron-withdrawing nature of the fused bithiazole monomers. The electrochemical bandgaps (E_g^{el}) of the copolymers were estimated from the cyclic voltammograms to be 1.77, 1.75, 1.69, and 1.62 eV for **P1**, **P2**, **P3,** and **P4**, respectively, which are in perfect agreement with the estimated UV-Vis spectra in thin film (E_g^{opt}).

Computational Calculations.

To investigate the effects of incorporating different heteroatoms on the geometries and frontier molecular orbitals (FMOS) of the synthesised polymers, theoretical calculations using density functional theory (DFT) at B3LYP/6-31G (d) was carried out as depicted in **Figure 3** and **Table S1**. To reduce the time for the calculations the alkyl side-chains in the polymer backbone where replaced by methyl groups and the calculations was carried out on dimer repeating units of the polymer. The data from the DFT findings revealed that both **P1** and **P2** have a highly planar backbone with a significantly small dihedral angle (ϑ_1- ϑ_3 = <0.02°) along the polymer backbone. This excellent planarity results from the intermolecular $S^{\delta+}\cdots N^{\delta-}$ and $N^{\delta-}\cdots H^{\delta+}$ between the nitrogen atoms of the fused

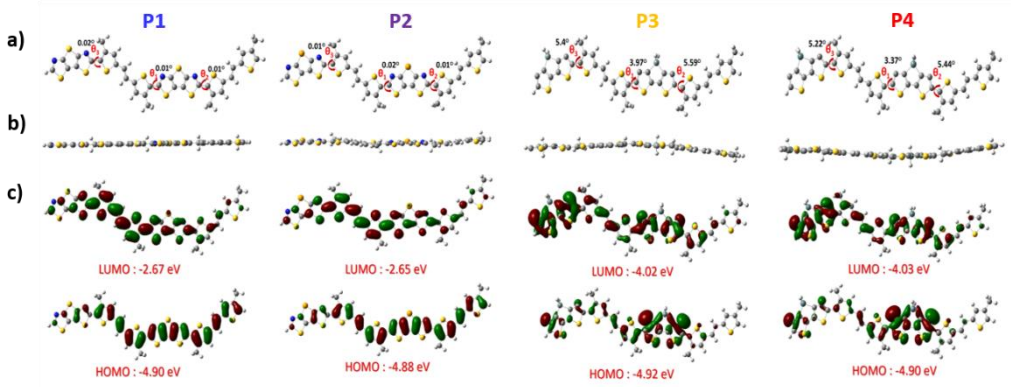

Figure 3. (a) Optimized molecular conformations front view, (b) side view and (c) frontier molecular orbitals of the dimer repeating units of the **P1**-**P4** calculated using Gaussian 09 simulations at the B3LYP/6-31G (d) level.

bithiazole and the adjacent TV unit.[67, 68] On the other hand, **P3** and **P4** showed a twisted backbone with ϑ_1- ϑ_3 = ~ 5° as a result, of the steric repulsion between the alkyl groups present on the heteroatoms in the fused bithiophene and TV units. As shown in **Figure 3c**, the FMOs of all the polymers where equally distributed along the molecular backbone; such extended conjugation can aid in effective electron/hole transport along the polymer backbone. The values of HOMO/LUMO of **P1**-**P4** were calculated to be -4.90/-2.67 eV, -4.88/-2.65 eV, -4.92/-4.02 eV and -4.90/-4.03 eV, respectively. Among **P1** *vs*. **P2** and **P3** *vs*. **P4**, the insertion of selenium and germanium atoms in **P2** and **P4** respectively, caused up-shifting of the FMO energy levels, which is ascribed from their higher electron-donating ability over the sulfur/silicon counterparts as reported previously (**P1** and **P3**, respectively).[69-71]

Organic Thin-Film Trransistor (OTFT) Measurements.

The UV-Vis absorption In order to study the influence of having a bridge atom in the fused bithiazole/dithiophene systems on TV-copolymers **P1-P4**, OTFT devices with a top-gate/bottom-contact (TG/BC) configuration were fabricated, as shown in **Figure 4a**. Gold and chromium-deposited borosilicate glass prepared by standard photolithiography methodologies were used as the drain/source

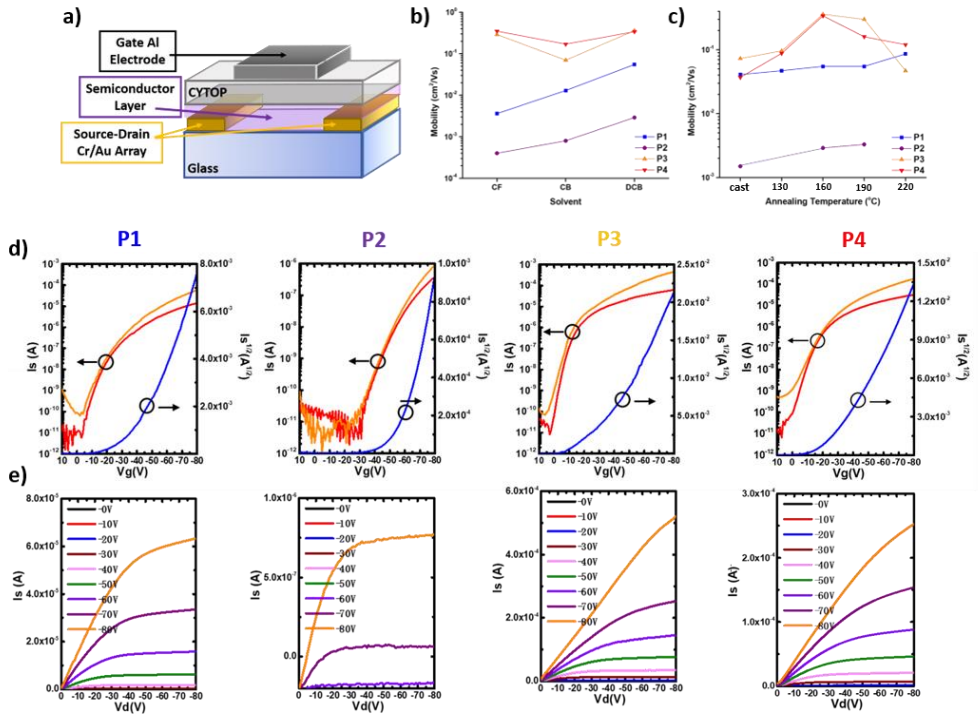

Figure 4. (a) Device configuration TG/BC. Device mobilities of copolymers **P1-P4** based OTFTs as a function of (b) copolymer solution solvent and (c) annealing temperature of the thin films. (d) Transfer and (e) output characteristics of TG/BC OTFTs devices based on semiconductor copolymers **P1-P4**.

electrode. The copolymer semiconducting layer was spin-coated from 5 mg/mL solutions of hot chloroform (CF), chlorobenzene (CB), or 1,2-dichlorobenzene (DCB), followed by the deposition of fluorinated polymer poly(perfluoroalkenyl vinyl ether) (CYTOP™) as the dielectric layer. The transistors were optimized by varying the copolymer solvent (**Figure 4b**) and temperature by thermally annealing the active layer (**Figure 4c**). Carrier mobilities (μ) and threshold voltage (V_{th}) were extracted from the linear and saturated regions in the transfer curves of the devices. On-off current ratio (I_{on}/I_{off}) of the optimal device performance for the copolymer semiconductors **P1-P4** are summarized in **Table 2**, and other performance parameters obtained under different conditions are presented in **Tables S2**-**S3**. The typical output and transfer plots for the best device performance based on **P1-P4** are depicted in **Figure 3d-e**.

A preliminary study was carried out by fabricating devices using different chlorinated solvents in the same concentration (5 mg/mL) deposited via spin-coating and annealed at 160 °C (**Table S2**). Interestingly, when changing the solvent from CF < CB < DCB, the device performance improved for the bithiazole-based **P1** and **P2** copolymers, while devices fabricated using dithiophene-based **P3** and **P4** copolymers presented similar performances when going from CF to DCB. However, it was slightly lower in CB for **P4**, but within the range, indicating only a small effect upon changing the solvent as depicted in **Figure 3b**. However, for **P3** using CB as the solvent was significantly lower in comparison to when using CF and DCB. This can be attributed to the increased threshold voltage (V_{th}). The value of V_{th} for **P3** in CF and DCB is only 26 V and 27 V, respectively, but increases to 41 V in CB (**Table S2**). The cause of such high V_{th} can be as result of carrier traps, interface barrier between the semiconductor and the insular, and the surface potential of the gate insulator. [72] In order to utilize the same solvent for all the copolymers, we decided to continue the device optimization using only 1,2-dichlorobenzene. In general, thermal annealing represents a successful method to optimize the device performance by facilitating the molecular orientation, enhancing film formation, improving crystallinity, and eliminating traces of residual solvent, which results in an increase in charge carrier transport. As depicted in **Figure 4c**, the annealing temperature (T_{an}) of the copolymer thin film plays a substantial role in the mobilities of all the copolymers. Devices based on the fused bithiazole unit exhibited direct temperature dependence as shown in **Table S3**. The maximum mobilities exhibited in as-cast devices were 0.041 cm^2/Vs for **P1** and 0.0015 cm^2/Vs for **P2** (**Table S3**), which were doubled to 0.086 cm^2/Vs for **P1** (T_{an} = 220 °C) and 0.0033cm^2/Vs for **P2** (T_{an} = 190 °C) upon annealing (**Table 2**). This demonstrates that increasing the annealing temperature, results in an enhanced chain arrangement with improved molecular order, and good overlap of donor-acceptor interactions, which improves the hole injection and charge transport. In comparison, devices fabricated from copolymers **P3** and **P4** exhibited the highest mobilities of 0.36 and 0.34 cm^2/Vs respectively (**Table 2**), at 160 °C, which is one order of magnitude higher than the results obtained for the corresponding as-casted devices 0.073 cm^2/Vs and 0.037 cm^2/Vs, respectively (**Table S2**). However, upon annulling the devices from 190 to 220 °C, the OTFT performance decreased, exhibiting mobilities of 0.30 and 0.047 cm^2/Vs for **P3,** and 0.16 to 0.12 cm^2/Vs for **P4**. Thus, illustrating the mobilities of copolymers are temperature dependent. In comparison, maximum mobilities of devices fabricated from fused dithiophene -based copolymers were higher than devices fabricated from bithiazole-based copolymers. The difference in mobilites can be attributed to the molecular weight and solubility of dithiophene-based copolymers **P3** and **P4**. In addition, the presence of bulky branched alkyl groups attached to the bridging central chalcogen germanium and silicon atoms, which is believed to lead to better film formation and advantageous for efficient charge transport in OFET devices.

Table 2. Electrical parameters of field-effect transistor devices based on copolymers **P1-P4**.

Materials	Annealing Temperature (°C)	μ_{Lin} (cm^2/Vs)		μ_{Sat} (cm^2/Vs)		V_{th} (V)	I_{On}/I_{off}
		Max	Avg	Max	Avg	Avg	
P1	220	0.060	0.049	0.086	0.069	43	10^6
P2	190	0.0022	0.0011	0.0033	0.0029	60	10^6
P3	160	0.096	0.075	0.36	0.17	27	10^6
P4	160	0.11	0.089	0.34	0.15	28	10^6

The substitution of the chalcogen bridge atom from sulfur to selenium in the fused bithiazole unit exhibited a strong effect on the device performance. A decrease of one order in magnitude was observed, which can be attributed to the lower-lying LUMO of **P1** (-3.61 eV) in comparison with **P2** (-3.59 eV). In contrast, this effect is not seen for the devices fabricated from copolymers containing the fused dithiophene system, which had similar mobility results for all the OTFT measurements. In addition, it is worth noting that the mobility obtained for **P4** is the highest to date that has been reported for such copolymers based on the DTG unit.[39, 54]

Molecular Packing and Crystallinity.

To further understand the molecular assembly and degree of crystallinity in the copolymer thin-films, grazing incidence wide angle X-ray spectroscopy (GIWAXS) was performed with a 2D detector. As observed in **Figure 5**, the copolymers were analyzed in the thin-film state annealed at 160 °C for 15 min. The dithiophene-based copolymers **P3** and **P4** showed a higher degree of crystallinity, in comparison to **P1** and **P2** based on the fused bithiazole moiety. Two clear lamellar reflections are discernible at 0.26 and 0.53 $Å^{-1}$ for **P1** and at 0.28 and 0.55 $Å^{-1}$ for **P2**, along with two perceptible π-π stacking reflections at 1.46 and 1.71 $Å^{-1}$ for **P1**, whereas only one reflection at 1.47 $Å^{-1}$ is observed for **P2**. Improved crystallinity was seen for TV-copolymers based on the dithiophene moiety with four

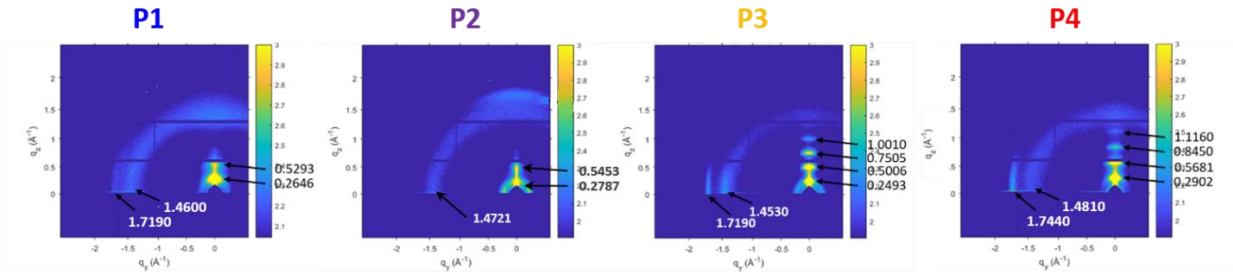

Figure 5. 2D-GIWAXS images of samples annealed at 160 °C of copolymers **P1**-**P4**.

lamellar reflections at 0.25, 0.50, 0.75, and 1.00 Å^{-1} for **P3** and at 0.29, 0.57, 0.85, and 1.12 Å^{-1} for **P4**. Two clear π-π stacking reflections for **P3** and **P4** were observed at 1.45, 1.72 Å^{-1} and 1.48, 1.74 Å^{-1}, respectively. These diffraction features in the out-of-plane direction suggest more ordered lamellar sheets for the dithiophene-based copolymers, whereas the reflections in the in-plane direction for **P1**, **P3,** and **P4** presented similar values indicating a more favorable "edge on" orientation and charge transport ability, which agrees with better performance obtained in OTFTs.[73-75] As summarized in **Table 1,** the d-spacing values for lower lamellar/π-π stacking reflections are **P1:** 11.86/3.67 Å, **P2:** 11.52/4.27 Å, **P3:** 6.28/3.65 Å, and **P4:** 5.61/3.61 Å, respectively. The copolymers containing the bithiazole unit **P1** and **P2** exhibited a lower degree of packing in comparison to the TV-copolymers based on the fused dithiophene unit **P3** and **P4**, which confirmed better packing in the solid-state.

Thin Film Morphology.

Investigating the morphological properties are important key parameter for the device performance; thus we have carried out the tapping mode atomic force microscope (AFM) in order to study the film morphologies of **P1**-**P4**. **Figure 6** presents the best topographic images (height and phase) of **P1**-**P4** films on SiO_2 at various annealing temperatures and as cast film (**Figure S7**) in DCB. Both fused bithiazole (**P1** and **P2**)- and dithiophene (**P3** and **P4**) of the polymer films exhibited finely aggregated surfaces, the root-mean-square (RMS) roughness values of as cast- and thermally annealed films are found to be **P1** = 1.16/1.15, **P2** = 0.53/0.59, **P3** = 0.80/0.90 and **P4** = 0.46/0.56 nm, respectively. They are no noticeable changes in the morphological features after thermal annealing of **P1** film at temperatures from 220 °C. On the other hand, thermally annealed polymer films **P2** at 190 °C, **P3** and **P4** (at 160 °C) showed marginally rougher surfaces compared to the as cast film (**Figure S7**). Thermal annealed film of the fused dithiophene-based polymers **P3** and **P4** not only lead to a fibrous domain but also resulted in the best device performances 0.36 and 0.34 cm^2/Vs, respectively. However, polymers **P1** and **P2** demonstrated some aggregated granular domains and resulted in poor device performances (0.06 and 0.003 cm^2/Vs). The poor device performances of **P1** and **P2** are likely due to the poor solubility or low molecular weight and low crystallinity. The significant increase in OTFT performances of the dithiophene-based copolymers **P3** and **P4** is due to the two ethyl-hexyl chains connected to the heteroatoms Si and Ge, which enables sufficient solution processability, higher crystallinity compared to **P1** and **P2,** that lack any flexible chains in the fused bithiazole core.

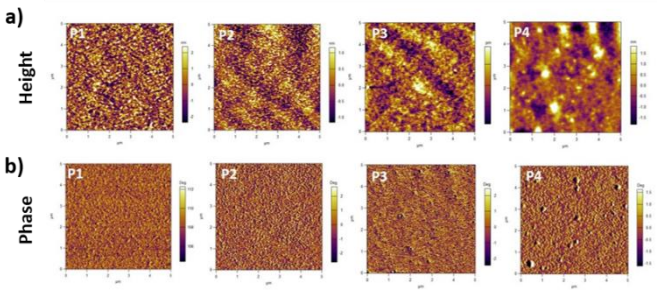

Figure 6. Tapping-mode AFM (a) height image and (b) phase image of as-cast films of copolymers **P1-4** and root-mean-square (RMS) roughness values **P1** = 1.16, **P2** = 0.53, **P3** = 0.80 and **P4** = 0.46 nm.

Conclusions

In conclusion, we have synthesized four novel thienylenevinylene copolymers **P1-P4** based on the bithiazole- and dithiophene-moieties via Stille coupling reaction. The copolymers have molecular weights in the range of 21-38 kDa, and Đ of 1.9-2.1, with high thermal stability (T_d > 300 °C) and low optical band gaps ranging from 1.67-1.74 eV. UV-Vis measurements demonstrate strong π-π stacking in solution and are more pronounced in the solid-state. Exchanging the chalcogen bridge atom from sulfur to selenium in the fused bithiazole unit or from Si to Ge in the dithiophene system results in a red-shifted absorption maximum. The HOMO/LUMO energy levels of **P1** and **P3**, were more stabilized in comparison to the copolymers **P2** and **P4**, having a larger central bridging atom. The annealing temperature demonstrated a strong influence on the OTFT device performance. With the best performance was observed in devices fabricated from copolymers based on dithiophene systems **P3** and **P4** exhibiting a maximum charge mobilities of 0.36 and 0.34 cm^2/Vs, respectively. Devices fabricated from the bithiazole-based copolymers **P1** and **P2** exhibited a maximum charge mobility of 0.09 and 0.003 cm^2/Vs, respectively. GIWAXS images show better packing for copolymers **P3** and **P4** with lower d-spacing values for lamellar and π-π stacking reflections. The findings demonstrate that the influence of the fused unit (bithiazole or dithiophene) systems and the type of bridging atom (S, Se, Si and Ge) have a profound influence

on the optoelectronic performance of low bandgap copolymer semiconductors.

Conflicts of interest

There are no conflicts to declare.

Acknowledgements

The authors gratefully acknowledge the support of this work from the Qatar National Research Fund (QNRF) and the National Priorities Research Program, project number NPRP10-0111-170152. Supported by Dr Joseph Strzalka, this research used resources of the Advanced Photon Source, a U.S. Department of Energy (DOE) Office of Science User Facility, operated for the DOE Office of Science by Argonne National Laboratory under Contract No. DE-AC02-06CH11357.

References

1. H. Bronstein, C. B. Nielsen, B. C. Schroeder and I. McCulloch, *Nature Reviews Chemistry*, 2020, **4**, 66-77.
2. S. Holliday, Y. Li and C. K. Luscombe, *Progress in Polymer Science*, 2017, **70**, 34-51.
3. L. Lu, T. Zheng, Q. Wu, A. M. Schneider, D. Zhao and L. Yu, *Chemical Reviews*, 2015, **115**, 12666-12731.
4. H. Sirringhaus, *Advanced Materials*, 2014, **26**, 1319-1335.
5. A. Facchetti, *Chemistry of Materials*, 2011, **23**, 733-758.
6. H. Dong, X. Fu, J. Liu, Z. Wang and W. Hu, *Adv Mater*, 2013, **25**, 6158-6183.
7. Y. Yamashita, F. Hinkel, T. Marszalek, W. Zajaczkowski, W. Pisula, M. Baumgarten, H. Matsui, K. Müllen and J. Takeya, *Chemistry of Materials*, 2016, **28**, 420-424.
8. F. Aniés, S. Wang, T. Hodsden, J. Panidi, Z. Fei, X. Jiao, Y. H. C. Wong, C. R. McNeill, T. D. Anthopoulos and M. Heeney, *Advanced Electronic Materials*, 2020, **6**, 2000490.
9. J. Panidi, A. F. Paterson, D. Khim, Z. Fei, Y. Han, L. Tsetseris, G. Vourlias, P. A. Patsalas, M. Heeney and T. D. Anthopoulos, *Advanced Science*, 2018, **5**, 1700290.
10. B. Sun, W. Hong, Z. Yan, H. Aziz and Y. Li, *Advanced Materials*, 2014, **26**, 2636-2642.
11. Y. Yuan, G. Giri, A. L. Ayzner, A. P. Zoombelt, S. C. B. Mannsfeld, J. Chen, D. Nordlund, M. F. Toney, J. Huang and Z. Bao, *Nature Communications*, 2014, **5**, 3005.
12. C. Luo, A. K. K. Kyaw, L. A. Perez, S. Patel, M. Wang, B. Grimm, G. C. Bazan, E. J. Kramer and A. J. Heeger, *Nano letters*, 2014, **14**, 2764-2771.
13. I. Kang, H.-J. Yun, D. S. Chung, S.-K. Kwon and Y.-H. Kim, *Journal of the American Chemical Society*, 2013, **135**, 14896-14899.
14. H. Huang, L. Yang, A. Facchetti and T. J. Marks, *Chemical Reviews*, 2017, **117**, 10291-10318.
15. X. Zhang, H. Bronstein, A. J. Kronemeijer, J. Smith, Y. Kim, R. J. Kline, L. J. Richter, T. D. Anthopoulos, H. Sirringhaus K. Song, M. Heeney, W. Zhang, I. McCulloch and D. M. Delongchamp, Nature communications, 2013, 4, 1-9.16. Y. He, W. Hong and Y. Li, *Journal of Materials Chemistry C*, 2014, **2**, 8651-8661.
17. M. Mas-Torrent and C. Rovira, *Chemical reviews*, 2011, **111**, 4833-4856.
18. K. Müllen and W. Pisula, *Journal of the American Chemical Society*, 2015, **137**, 9503-9505.
19. M. Comí, M. U. Ocheje, S. Attar, A. U. Mu, B. K. Philips, A. J. Kalin, K. E. Kakosimos, L. Fang, S. Rondeau-Gagné and M. Al-Hashimi, *Macromolecules*, 2020, DOI: 10.1021/acs.macromol.0c02021.
20. M. Barłóg, X. Zhang, I. Kulai, D. S. Yang, D. N. Sredojevic, A. Sil, X. Ji, K. S. M. Salih, H. S. Bazzi, H. Bronstein, L. Fang, J. Kim, T. J. Marks, X. Guo and M. Al-Hashimi, *Chemistry of Materials*, 2019, **31**, 9488-9496.
21. D. Hashemi, X. Ma, R. Ansari, J. Kim and J. Kieffer, *Physical Chemistry Chemical Physics*, 2019, **21**, 789-799.
22. Y. Wang and T. Michinobu, *Journal of Materials Chemistry C*, 2018, **6**, 10390-10410.
23. K. Schmoltner, F. Schlütter, M. Kivala, M. Baumgarten, S. Winkler, R. Trattnig, N. Koch, A. Klug, E. J. List and K. Müllen, *Polymer Chemistry*, 2013, **4**, 5337-5344.
24. X. Guo, A. Facchetti and T. J. Marks, *Chemical reviews*, 2014, **114**, 8943-9021.
25. H. L. Su, D. N. Sredojevic, H. Bronstein, T. J. Marks, B. C. Schroeder and M. Al-Hashimi, *Macromolecular rapid communications*, 2017, **38**, 1600610.
26. Y. Wang and T. Michinobu, *Journal of Materials Chemistry C*, 2016, **4**, 6200-6214.
27. Z. Zeng, Y. Li, J. Deng, Q. Huang and Q. Peng, *Journal of Materials Chemistry A*, 2014, **2**, 653-662.
28. S. Vegiraju, G.-Y. He, C. Kim, P. Priyanka, Y.-J. Chiu, C.-W. Liu, C.-Y. Huang, J.-S. Ni, Y.-W. Wu, Z. Chen, G.-H. Lee, S.-H. Tung, C.-L. Liu, M.-C. Chen and A. Facchetti, *Advanced Functional Materials*, 2017, **27**, 1606761.
29. S.-Y. Jang, I.-B. Kim, J. Kim, D. Khim, E. Jung, B. Kang, B. Lim, Y.-A. Kim, Y. H. Jang, K. Cho and D.-Y. Kim, *Chemistry of Materials*, 2014, **26**, 6907-6910.
30. H.-L. Su, D. N. Sredojevic, H. Bronstein, T. J. Marks, B. C. Schroeder and M. Al-Hashimi, *Macromolecular Rapid Communications*, 2017, **38**, 1600610.
31. D. Patra, J. Lee, S. Dey, J. Lee, A. J. Kalin, A. Putta, Z. Fei, T. McCarthy-Ward, H. S. Bazzi, L. Fang, M. Heeney, M.-H. Yoon and M. Al-Hashimi, *Macromolecules*, 2018, **51**, 6076-6084.
32. Z. Yuan, B. Fu, S. Thomas, S. Zhang, G. DeLuca, R. Chang, L. Lopez, C. Fares, G. Zhang, J.-L. Bredas and E. Reichmanis, *Chemistry of Materials*, 2016, **28**, 6045-6049.
33. Y. Teshima, M. Saito, T. Fukuhara, T. Mikie, K. Komeyama, H. Yoshida, H. Ohkita and I. Osaka, *ACS Applied Materials & Interfaces*, 2019, **11**, 23410-23416.
34. S.-Y. Jang, I.-B. Kim, M. Kang, Z. Fei, E. Jung, T. McCarthy-Ward, J. Shaw, D.-H. Lim, Y.-J. Kim, S. Mathur, M. Heeney and D.-Y. Kim, *Advanced Science*, 2019, **6**, 1900245.
35. B. Walker, D. Han, M. Moon, S. Y. Park, K.-H. Kim, J. Y. Kim and C. Yang, *ACS Applied Materials & Interfaces*, 2017, **9**, 7091-7099.
36. E. Collado-Fregoso, P. Boufflet, Z. Fei, E. Gann, S. Ashraf, Z. Li, C. R. McNeill, J. R. Durrant and M. Heeney, *Chemistry of Materials*, 2015, **27**, 7934-7944.
37. V. Gupta, L. F. Lai, R. Datt, S. Chand, A. J. Heeger, G. C. Bazan and S. P. Singh, *Chemical Communications*, 2016, **52**, 8596-8599.

38. A. Casey, S. D. Dimitrov, P. Shakya-Tuladhar, Z. Fei, M. Nguyen, Y. Han, T. D. Anthopoulos, J. R. Durrant and M. Heeney, *Chemistry of Materials*, 2016, **28**, 5110-5120.
39. Z. Fei, J. S. Kim, J. Smith, E. B. Domingo, T. D. Anthopoulos, N. Stingelin, S. E. Watkins, J.-S. Kim and M. Heeney, *Journal of Materials Chemistry*, 2011, **21**, 16257-16263.
40. H.-C. Chen, Y.-W. Su and K.-H. Wei, *Journal of Materials Chemistry A*, 2016, **4**, 2228-2235.
41. H. Huang, J. Youn, R. Ponce Ortiz, Y. Zheng, A. Facchetti and T. Marks, *Chemistry of Materials*, 2011, **23**, 2185-2200.
42. W. Kang, M. Jung, W. Cha, S. Jang, Y. Yoon, H. Kim, H. J. Son, D.-K. Lee, B. Kim and J. H. Cho, *ACS applied materials & interfaces*, 2014, **6**, 6589-6597.
43. B. Nketia-Yawson, A.-R. Jung, Y. Noh, G.-S. Ryu, G. D. Tabi, K.-K. Lee, B. Kim and Y.-Y. Noh, *ACS Applied Materials & Interfaces*, 2017, **9**, 7322-7330.
44. Z. Fei, M. Shahid, N. Yaacobi-Gross, S. Rossbauer, H. Zhong, S. E. Watkins, T. D. Anthopoulos and M. Heeney, *Chemical Communications*, 2012, **48**, 11130-11132.
45. H. Zhong, Z. Li, F. Deledalle, E. C. Fregoso, M. Shahid, Z. Fei, C. B. Nielsen, N. Yaacobi-Gross, S. Rossbauer, T. D. Anthopoulos, J. R. Durrant and M. Heeney, Journal of the American Chemical Society, 2013, 135, 2040-2043.
46. H. Zhong, Z. Li, E. Buchaca-Domingo, S. Rossbauer, S. E. Watkins, N. Stingelin, T. D. Anthopoulos and M. Heeney, *Journal of Materials Chemistry A*, 2013, **1**, 14973-14981.
47. Q. Wang, S. Zhang, L. Ye, Y. Cui, H. Fan and J. Hou, *Macromolecules*, 2014, **47**, 5558-5565.
48. O. Kwon, S. Park, J. K. Park and D. Hwan Wang, *Dyes and Pigments*, 2018, **158**, 233-239.
49. Z. Wang, X. Li, Y. Zou, J. Tan, X. Fu, J. Liu, C. Xiao, H. Dong, W. Jiang, F. Liu, Y. Zhen, Z. Wang, T. P. Russel and W. Hu, Journal of Materials Chemistry C, 2016, 4, 7230-7240
50. M. Jung, Y. Yoon, J. H. Park, W. Cha, A. Kim, J. Kang, S. Gautam, D. Seo, J. H. Cho, H. Kim, J. Y. Choi, K. H. Chae, K. Kwak, H. J. Son, M. J. Ko, H. Kim, D. K. Lee, J. Y. Kim, D. H. Choi and B. S. Kim, ACS nano, 2014, 8, 5988-6003.
51. K.-H. Kim, H. Yu, H. Kang, D. J. Kang, C.-H. Cho, H.-H. Cho, J. H. Oh and B. J. Kim, *Journal of Materials Chemistry A*, 2013, **1**, 14538-14547.
52. S.-H. Kang, J. Lee, D. Yoo, B. H. Lee and C. Yang, *Journal of Materials Chemistry C*, 2019, **7**, 8522-8526.
53. M. J. Kim, M. Jung, W. Kang, G. An, H. Kim, H. J. Son, B. Kim and J. H. Cho, *The Journal of Physical Chemistry C*, 2015, **119**, 16414-16423.
54. A. Casey, Y. Han, Z. Fei, A. J. P. White, T. D. Anthopoulos and M. Heeney, *Journal of Materials Chemistry C*, 2015, **3**, 265-275.
55. J. Ohshita, Y. Adachi, R. Sagisaka, M. Nakashima, Y. Ooyama and Y. Kunugi, *Synthetic Metals*, 2017, **227**, 87-92.
56. B. Lim, K. J. Baeg, H. G. Jeong, J. Jo, H. Kim, J. W. Park, Y. Y. Noh, D. Vak, J. H. Park , J. W. Park and D. Y. Kim, Advanced Materials, 2009, 21, 2808-2814.
57. S.-Y. Jang, I.-B. Kim, J. Kim, D. Khim, E. Jung, B. Kang, B. Lim, Y.-A. Kim, Y. H. Jang, K. Cho and D. Y. Kim, Chemistry of Materials, 2014, 26, 6907-6910.
58. M. Al-Hashimi, M. A. Baklar, F. Colleaux, S. E. Watkins, T. D. Anthopoulos, N. Stingelin and M. Heeney, *Macromolecules*, 2011, **44**, 5194-5199.
59. D. Patra, J. Lee, J. Lee, D. N. Sredojevic, A. J. White, H. S. Bazzi, E. N. Brothers, M. Heeney, L. Fang , M.-H. Yoon and M. Al-Hashimi, Journal of Materials Chemistry C, 2017, 5, 2247-2258.
60. D. Patra, J. Lee, S. Dey, J. Lee, A. J. Kalin, A. Putta, Z. Fei, T. McCarthy-Ward, H. S. Bazzi, L. Fang, M. Heeney, M. H. Yoon and M. Al-Hashimi, Macromolecules, 2018, 51, 6076-6084.
61. J. Ohshita, Y.-M. Hwang, T. Mizumo, H. Yoshida, Y. Ooyama, Y. Harima and Y. Kunugi, *Organometallics*, 2011, **30**, 3233-3236.
62. J. S. Kim, Z. Fei, D. T. James, M. Heeney and J.-S. Kim, *Journal of Materials Chemistry*, 2012, **22**, 9975-9982.
63. A. J. Musser, M. Al-Hashimi, M. Heeney and J. Clark, *The Journal of chemical physics*, 2019, **151**, 044902.
64. Y.-A. Kim, Y.-J. Jeon, M. Kang, S.-Y. Jang, I.-B. Kim, D.-H. Lim, Y.-J. Heo and D.-Y. Kim, *Organic Electronics*, 2017, **46**, 77-87.
65. C. M. Amb, S. Chen, K. R. Graham, J. Subbiah, C. E. Small, F. So and J. R. Reynolds, *Journal of the American Chemical Society*, 2011, **133**, 10062-10065.
66. N.-K. Kim, S.-Y. Jang, G. Pace, M. Caironi, W.-T. Park, D. Khim, J. Kim, D.-Y. Kim and Y.-Y. Noh, *Chemistry of Materials*, 2015, **27**, 8345-8353.
67. J. Wu, Q. Fan, M. Xiong, Q. Wang, K. Chen, H. Liu, M. Gao, L. Ye, X. Guo, J. Fang, Q. Guo, W. Su, Z. Ma, Z. Tang, E. Wang, H. Ade and M. Zhang, *Nano Energy*, 2021, **82**, 105679.
68. G. P. Kini, J. Y. Choi, S. J. Jeon, I. S. Suh and D. K. Moon, *Polymer Chemistry*, 2019, **10**, 4459-4468.
69. L. Zhong, H. Bin, I. Angunawela, Z. Jia, B. Qiu, C. Sun, X. Li, Z. Zhang, H. Ade and Y. Li, *Macromolecules*, 2019, **52**, 4776-4784.
70. J. Liu, J. Ren, S. Zhang and J. Hou, *Polymer Chemistry*, 2020, **11**, 5019-5028.
71. M. Nakashima, M. Miyazaki, Y. Ooyama, Y. Fujita, S. Murata, Y. Kunugi and J. Ohshita, *Polymer Journal*, 2016, **48**, 645-651.
72. Y.-H. Kim, Y. U. Lee, J.-I. Han, S.-M. Han and M.-K. Han, *Journal of the Electrochemical Society*, 2007, **154**, H995.
73. D.-Y. Chiou, Y.-C. Su, K.-E. Hung, J.-Y. Hsu, T.-G. Hsu, T.-Y. Wu and Y.-J. Cheng, *Chemistry of Materials*, 2018, **30**, 7611-7622.
74. X. Gong, G. Li, Y. Wu, J. Zhang, S. Feng, Y. Liu, C. Li, W. Ma and Z. Bo, *ACS applied materials & interfaces*, 2017, **9**, 24020-24026.
75. K. W. Song, M. H. Choi, H. J. Song, S. W. Heo, J. Y. Lee and D. K. Moon, *Solar energy materials and solar cells*, 2014, **120**, 303-309.